The effect of Anisotropy, due Macroscopic Strain and Bfield incident angle on YBCO strip's critical temperature T_C

R. Bentley
L3 Advanced Labs, Lab Group Condensed Matter, Lab Day

The anisotropy of commercial YBCO was proven by varying the angle between incident B field and the Copper oxide planes. It showed the two-dimensionality of YBCO's superconductivity. The T_c decreased from (90.9±0.5)K to (89.8±0.6)K when the B field was at a Maxima. Macroscopic strains were applied on 3d printed bridges in No field and T_c did not change. When a B field was applied to the highest strain the T_c became (88.8±0.5)K. B field intensity on CuO_2 has a negative correlation to T_c. The degrees of freedom in the experiment where reduced and showed that the largest contribution to error was the angle between the B field and the Copper oxide plane. BCS theory and the modern take on cuprate superconductivity was discussed

Submitted: TODAY, Date of Experiment: EXPERIMENT DATE

1. Introduction

In 1908, Onnes was first to liquefy helium and received the nobel prize in 1913[1]. Onnes then started investigating the electrical resistance of pure metals at low temperatures. He first experimented with pure mercury and observed a steady decrease in its electrical resistance when it was cooled. To his surprise the resistance had become negligible when it was cooled below 4.2K[1][2], this temperature would later be called the critical temperature of Mercury. This implied that the solid mercury had achieved a state with significantly higher conductivity. Onnes named this phenomenon superconductivity and motivated a new area of physics. Onnes ran the only laboratory at the time to produce liquid helium. Liquid helium is very expensive, so the race to discover higher temperature superconductors began. The Superconductive phase is only prevalent in specific materials, with temperatures lower than their critical temperature. It is a reversible process. The critical temperature is an intrinsic property of a superconducting material. Another important characteristic of superconductors are their magnetic properties. The magnetic properties of superconductors were discovered in 1933 by Meissner. The Meissner effect states that in the superconducting phase the superconductor expels applied magnetic fields, B field[3]. This was justified by its theoretical infinite conductivity. When the incident B field is increased, small currents occur within the superconductor that oppose the change in induction within it, by Lenz's law. In a normal metallic structure, the energy of the induced currents will dissipate due to the metal's resistance, however for a superconductor theoretically it has no resistance. This implies that the induced currents, within a superconductor, will not decay. The overall B field strength will remain zero within a superconductor. In practicality the conductivity in the superconductor phase is very large and not infinite. The B field within a material is given by eq(1)[3]

$$B = \mu_0(H + M) \qquad \text{eq(1)}$$

Using the derivation in Supplementary Appendix 1 it can be shown that the magnetic susceptibility χ of a superconductor is -1. This implies that superconductors that obey the Meissner effect display perfect diamagnetism. Diamagnetism aims to lower the strength of its intrinsic B field[3].An important breakthrough in superconductivity was the development of BCS theory[4]. It was named after the pioneer physicists Bardeen, Cooper and Schrieffer who were awarded the Nobel prize in 1972 for their collective contributions. The theory proposes the existence of Cooper pairs. Cooper pairs provide a model which describes the origin of the superconductivity. The typical superconductor, at the time of this theories discovery, was thought of as having a neatly arranged structure of positive cations (or metal ions) with a sea of delocalised electrons, an isomorphic material. A physicist's description would be that the superconductor would have a periodic crystal structure. The delocalised sea of fermions arises from the outer orbitals fusing. Fermions are spin half-integer particles, which obey the Pauli exclusion principle.
These fermions occupy the lowest energy eigenstates, these electrons cannot occupy the same energy eigenstates simultaneously, so they are single electron eigenstates. In the superconducting phase a pair of electrons form a bound symmetric state due to an attractive interaction caused by crystal vibrations [5]. An exchange of virtual phonons causes this attractive interaction between the two electrons in the cooper pair. This interaction overcomes the strong coulomb potential. If this attraction is weak the cooper pairs will breakdown and the coulomb repulsion will dominate this interaction[5]. When this superconductive material is cooled below its critical temperature the entropy of the system decreases. During the transition the fermionic half spin electrons form zero spin cooper pairs, because the coupled pair of electrons have opposite spins.
The superconducting phase breaks down when an applied magnetic field strengths exceed the critical field strength, even when the temperature is lower than the critical temperature. This is an intrinsic value for the type of superconductors discussed so far called type 1. The transition between the superconducting and normal phases is discrete, nearly instant. It was shock to the scientific community in 1933 when a second type of superconductor was discovered. The type 2 superconductor has two critical fields[5]. Type II behave like type I superconductors when the applied field is less that their first critical field. However, if an increasing magnetic field is applied, once the first critical field is exceeded and the field strength continues increasing there is a gradual continuous transition, from a superconducting state to a normal state called a mixed state[3]. This mixed state allows some field lines to penetrate the superconductor through thin filaments, which are parallel to the field. Figure 1 shows this phase

transition. Currents will circulate around the perimeters of these filaments and these parts of the superconductor will return to the normal state. They are called vortices[6]. The type II will still display superconductive properties in this state. When the applied field exceeds the second critical field they are no longer in a superconducting phase.

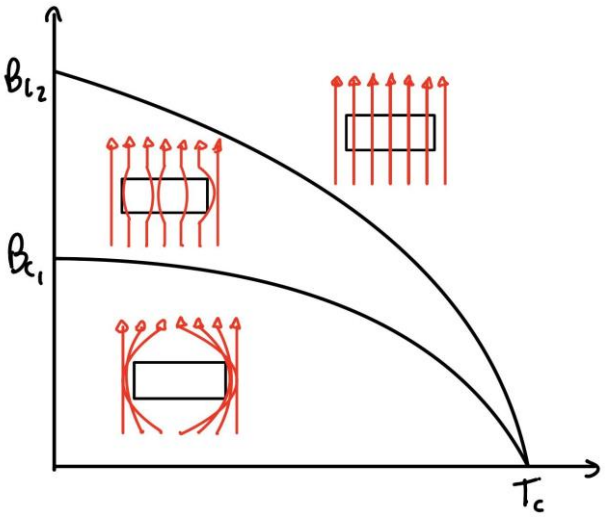

Figure 1: Shows the different phases of a type II superconductor in a varying B field.

YBCO is a Type II superconductor. In this experiment the B field used exceeds the magnitude of the first critical field. In 1986 superconductivity was observed in cuprates, copper oxides. The critical temperatures were higher than any previously recorded (35K) and the Nobel prize was awarded in 1987 to Bednorz and Muller for the investigation of ceramic high temperature superconductors[7]. A year later in 1988, Maw-Kuen Wu and Chu Ching-wu discovered the first superconductor with a critical temperature higher than liquid nitrogen (77K)[7]. $YBa_2Cu_3O_7$ had a critical temperature of 93K[2]. This allowed the study of superconductivity to become cheaper[1][2]. liquid nitrogen is cheaper than liquid helium and it easier to store. The problem with ceramic superconductors was their disagreement with the well-established BCS theory[8]. Mercury, which was mentioned briefly before, has an isomorphic metallic structure, and has superconductivity in all planes.
YBCO's structure is shown in figure 2. It consists of CuO_2 planes and Y and Ba dopants, which distort the symmetry of the Copper oxide planes, and cause superconductivity. YBCO does not obey BCS theory[9].

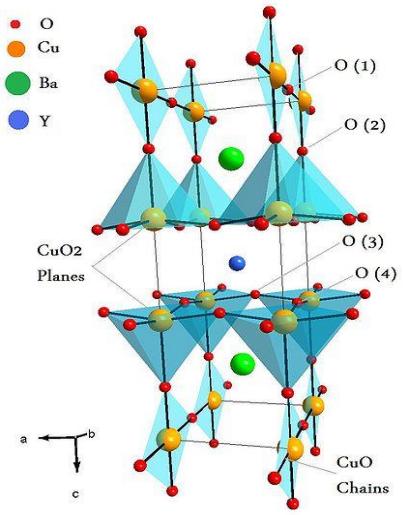

Figure 2: shows the structure of YBCO[9]

A true understanding of high temperature superconductivity is yet to be established and remains controversial. BCS theory will be adjusted slightly to justify the findings of this report. The cooper pairs will now be referred to as quasi-particles[10], to avoid controversy. This report will investigate the anisotropy of YBCO[11]. Anisotropy is a directional property of a material. There are delocalised electrons present in the copper oxide plane and this plane experiences a higher level of superconductivity than the other directions. An incident B field, with a magnitude between YBCO's critical fields, will be applied at various angles to this highly superconductive plane. This will cause different amounts of vortices production[10]. Also, a macroscopic strain will be applied to the commercial YBCO, to investigate the bulk properties of the commercial tape.

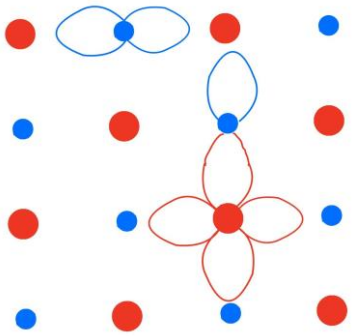

Figure 3: shows the structure of a Copper oxide plane. The red circles are copper atoms and blue circles are oxygen atoms.

Figure 3 shows a rough illustration of the Copper oxide plane. The 3d orbitals of the Cu overlap with the 2p orbitals of the oxygen[11]. When the CuO_2 is not doped it is an antiferromagnet and mott insulator[12]. Because neighbouring copper atoms will have opposite spins and electrons in the covalent bonds are localised and trapped by a strong coulomb repulsion. The electrons cannot jump between Cu sites they can only interact over the pi orbital. In YBCO the presence of dopants breaks the symmetry by providing hole to the system. The 2p orbital and 3d orbital electrons of the oxygen and copper in the YBCO structure are not necessarily free, but they can

move between sites, because the hole melts the anti-ferromagnetism.

2. Method

The equipment used in this experiment was: a cryostat, electromagnetic coils, Glassman, mercury ITC, Keithley 2000s, experimental stick, platinum thermometer, hall probe, power sources and a commercial YBCO strip.

Firstly, a platinum thermometer, hall probe and a commercial YBCO strip we soldered and wired to Keithley 2000s, which act as multimeters, to form the circuits shown in Supplementary Appendix 2.

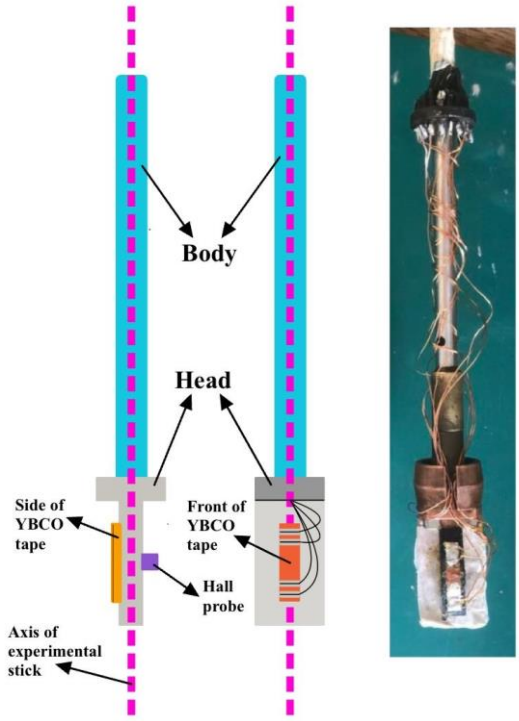

Figure 4: shows the components of the experiment stick, on the right the YBCO is vanished to a bridge.

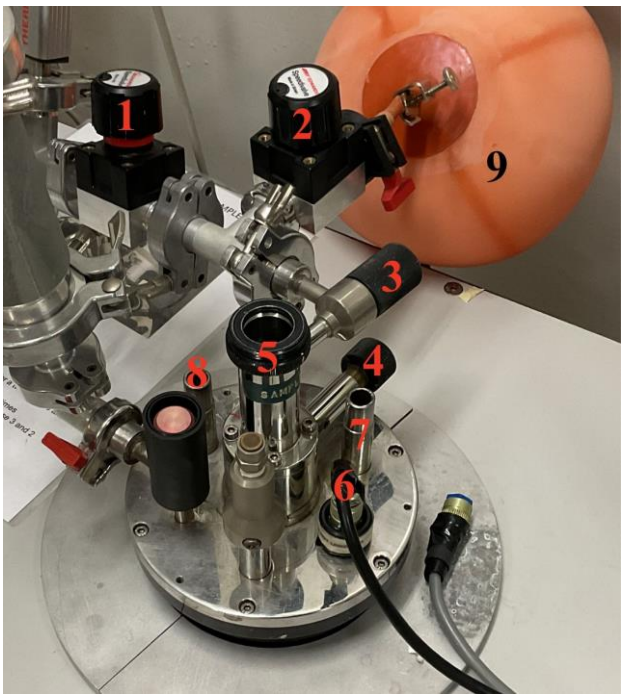

Figure 5: shows components of cryostat.

The experimental stick was placed down in the 5, shown above, and was sealed with a clamp. The cryostat was flushed before liquid nitrogen is added. The extraction pump was turned on to extract water molecules from the air in the chamber, because if liquid nitrogen was added straight away the water would have frozen in the tubes and caused various systematic errors and problems. The extraction pump was isolated from the helium source 9 and kept on until the pressure of the chamber reached approximately 10^{-2} mbar. After this 1 was closed, which cut the pump off from the chamber and 2 was opened which allowed the helium reservoir to fill the chamber for two seconds and then 2 was closed. This process was repeated three times. On the final time 1 was closed and 2 was opened to create a helium environment, 3 was closed and 2 was closed two seconds after. 1 was opened to evacuate the chamber and then finally the vacuum pump was switched off. At the end of these steps the chamber was now evacuated with a helium environment.

The experimental chamber was cooled, by pouring liquid nitrogen in a funnel leading into 7 at a steady rate. It was poured in with a steady rate so it didn't splash out or large quantities of it evaporated. Gloves and goggles were worn for protection against the cold 77K liquid nitrogen.

LabVIEW software was used to control the Mercury ITC, Glassman and Keithley. The Keithley's in the arrangement shown in Supplementary Appendix 2 exported live data to the LabView, with the highest sample rate. This exportation of data was displayed on a monitor and the decrease in temperature, measured by the Mercury ITC's calibrated thermometer, was shown in a live chart.

Simultaneously, two power sources were used to generate a current of 110mA through the Sample and a 50mA current through the thermometer. Once the system had reached a near static equilibrium at around 77K, the Mercury ITC was told by the LabVIEW to apply a constant power. 4 in figure 5 is the gate to liquid nitrogen reservoir to the chamber of the experimental stick.

In the early experiments a 20 percent power was used with the liquid nitrogen reservoir being fully closed. The temperature would climb steadily and the live data recorded would be exported to an excel spreadsheet. The heating was applied until the YBCO had fully transitioned back into the normal state. Once this had happened the heating was turned off and 4 was opened again to cool the chamber. This process could be repeated multiple times. The transition normally lasted around 30 seconds.

In later experiments a 5 percent heating was applied, with the liquid nitrogen reservoir being partially open. There was a dynamical equilibrium between the liquid nitrogen that was being applied and the heating, this required great technique.

This technique would show a slow and steady 10-minute transition with lots of data. The 20 percent method was still used, even in later experiments, because it was a quicker experiment and made it easier to collect repeats.

After a day's experiments where completed, the liquid nitrogen reservoir was left open and allowed to evaporate. The resistance of the platinum thermometer and the temperature of the Mercury ITC were recorded overnight. The platinum thermometer is temperature sensitive device and the temperature in the chamber was

modelled as a function of its resistance. This model is a 4th order polynomial of resistance and was curve fitted to the mercury ITC's temperature for a temperature range between 80-100K, because the critical temperature is around 92K. Below shows this model[13].

$$T(R) = a_0 + a_1R + a_2R^2 + a_3R^3 + a_4R^4 \quad \text{eq(2)}$$

The errors associated with these models are discussed in Error Appendix 1 and Error Appendix 2.

The anisotropy of the YBCO was investigated by applying a strong magnetic field to it. The YBCO's superconductivity is dominated by the Copper oxide planes, so the incident B field was varied on the surface of the YBCO strip to see this anisotropy. The following angles where used $\phi = 0^o, 30^o, 45^o$ and 90^o. ϕ is defined in the figure below.

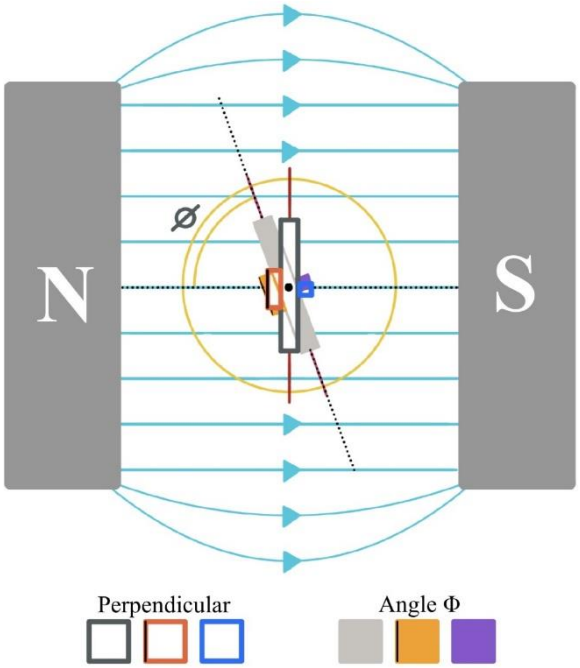

Figure 6: Illustration of the Birdseye view above the experimental stick between a uniform B field. There are two cases shown, one perpendicular and one subtended at an angle of ϕ between the B field and the axis of the experimental stick. The key identifies which component belongs to each case. The Grey larger rectangles represent the bodies of the experimental sticks. The orange rectangles represent the YBCO strips in each case, and the black line denotes It's "top" face. The blue and purple cubes represent the Hall probes for each case.

The top face of the YBCO lays on top of the substrate which will be talked about later in this report. The angles were calculated using the voltage recorded by the hall probe. When the probe was rotated around the axis of the experimental stick it gave a sinusoidal voltage curve, as expected. The specific voltages to achieve ϕ angles are given by the equation below.

$$V = V_{max}\cos(\phi) \quad \text{eq(3)}$$

Details on removing the noise errors are given in Error Appendix 3 and the B field was generated with a Glassman setting of ISET 20: VSET 50, which gives the strongest possible applied field.

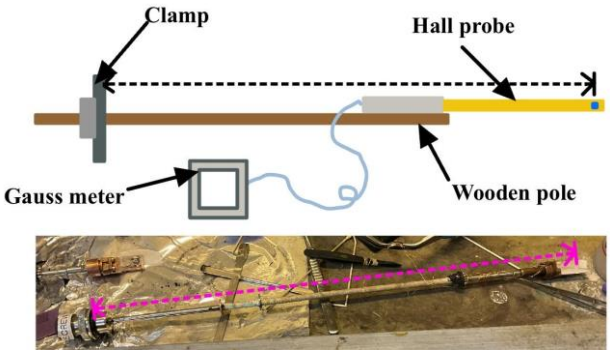

Figure 7: shows a schematic diagram for the Gauss stick, the active lengths (dotted lines) are equal in length, 52.5cm

A Gauss stick was used to test the behaviour of the magnetic field lines between the coils, as the core surrounding the experimental stick was iron and the experimental stick did not lie equidistant between the coils. The gauss stick had the same active length as the experimental stick, so its hall probe on the attached gaussmeter would lay in the same position as the experimental stick's Hall probe would inside the Chamber. When it was placed in the chamber the coils had their experimental setting of ISET: 20A VSET 50V. The gauss stick was moved in different directions and turned 180 degrees to observe two different maxima and verified that the fields where uniform. The largest maxima was called V_{max} which was used in the angle equation referenced before.

The B field angle experimental method used the same techniques referenced before, but the experimental stick was positioned at different angles under a strong B field.

More details about the errors associated with angles are in the Error Appendix 4. The final layer of complexity added to the experiment was a macroscopic strain. This strain was applied through a 3d printed bridge.

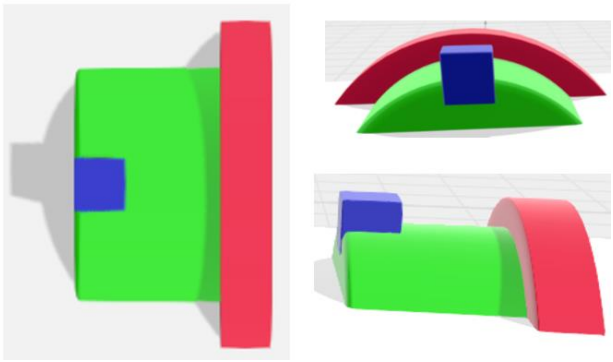

Figures 8(left), 9(upper right) and 10(lower right): are schematic diagrams for the structure of the bridges from different perspectives. The three key segments are coloured. The green segment is the arch; the red segment is the rail and the blue segment is the modified rail.

In this experiment two bridges where tested.

To attach the YBCO to the bridge it must be varnished. The normal varnishing method can be seen in Supplementary Appendix 3. The modified method is shown in the image below.

Figure 11: shows the varnishing technique for the Bridge experiments.

The same vanish steps apply, however there is an additional vanish step when resting the YBCO tape on top of the bridge. It is held in place by pliers, so the YBCO does not slip out of the central position.
The bridge also undergoes the varying angle B field experiment. There was not a lot of time near the end of this experiment, so the angles were marked with white markers, so the experimental stick could be positioned faster. The errors associated with this method are talked about in Error Appendix 4A.

After the data was collected transition gradients of the R vs T graphs, where curve-fitted with double gaussians. The different variations in experiment displayed unique properties for these gaussians. To overcome the noise produced by the experiment a rolling average of three was chosen to filter the Sample Resistance and Platinum Thermometer Temperature datasets[14].

$$\frac{dR}{dT} = a_1 e^{-\frac{(T-\mu_1)^2}{2\sigma_1^2}} + a_2 e^{-\frac{(T-\mu_2)^2}{2\sigma_2^2}} \qquad \text{eq(4)}$$

This was done to calculate the critical temperature of YBCO in each experiment. The gradient displayed two gaussians, the average of the means μ would give the critical temperature

$$T_c = \frac{\mu_1+\mu_2}{2} \qquad \text{eq(5)}$$

The error of the critical temperature was calculated in Error Appendix 4.

Bridge	Radius of Curvature
Bridge 1	(13.9 ± 0.1)mm
Bridge 2	(20.1 ± 0.1)mm

Table 1: Shows the radius of curvatures for the arc segments of the respective bridges

Two tests were used to find the biggest contribution to B field error. They were the Knock test and repositioning test. For the repositioning test the corrected maxima (perpendicular angle) is recorded and a white line is marked on the black clamp attached to 5 on the cryostat in figure 6. The experimental stick is rotated out of position and it repositioned to the original mark. There is an error in the repositioning is addressed in Error Appendix 5A.

The knock test was performed when the YBCO was laying on the first bridge. The maxima (perpendicular position) voltage was recorded and then the table housing the cryostat was given a harsh nudge. The difference between the new and old maxima gave the error in the angles order of magnitude if someone nudged table accidently during the experiment. The maximum voltages where averages. An in depth description is in Error Appendix 5B.

3. Results

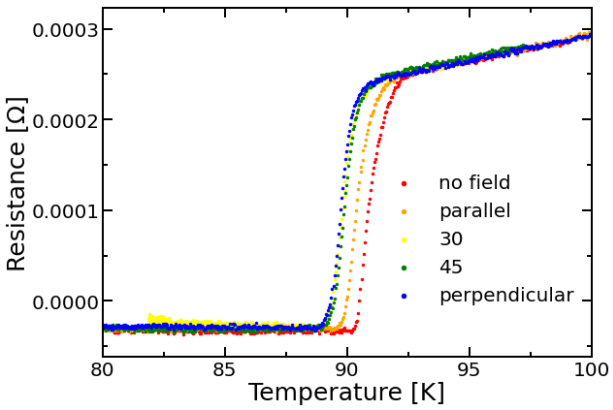

Figure 12: Shows the transition of the zero strain YBCO into the superconducting phase for different B field incident angles.

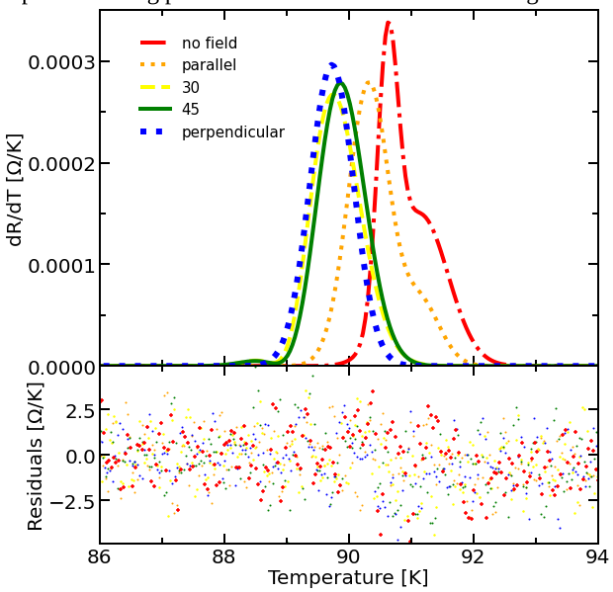

Figure 13: Shows the gradient of the no strain transition, curve-fitted to the double gaussian model, note the residuals are multiplied by 10^5

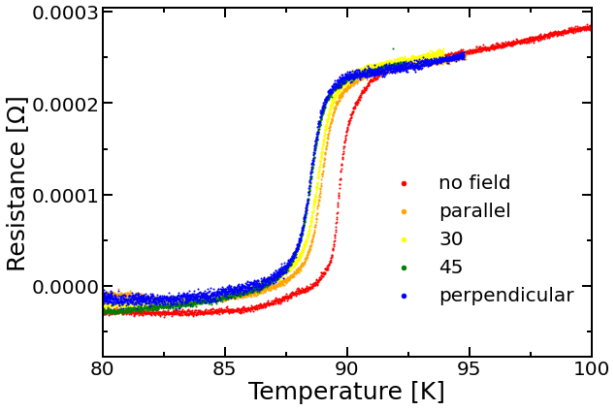

Figure 14: Shows the transition for the YBCO, on the first bridge, into the superconducting phase for different B field incident angles.

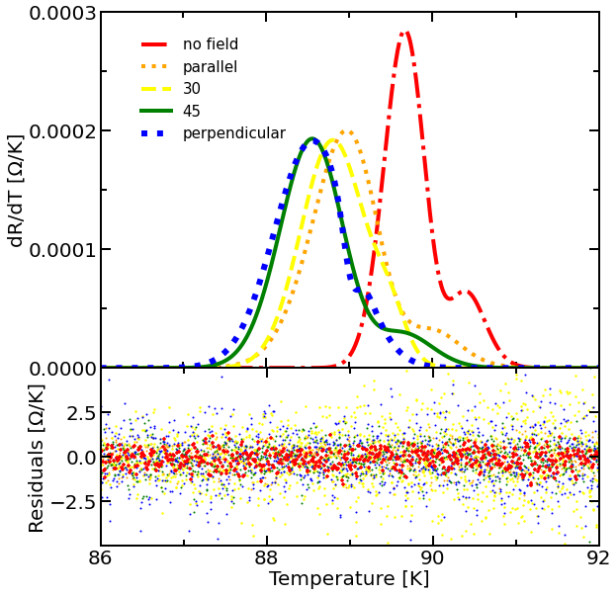

Figure 15: Shows the gradient of transition for the first bridge, curve-fitted to the double gaussian model, note the residuals are multiplied by 10^4

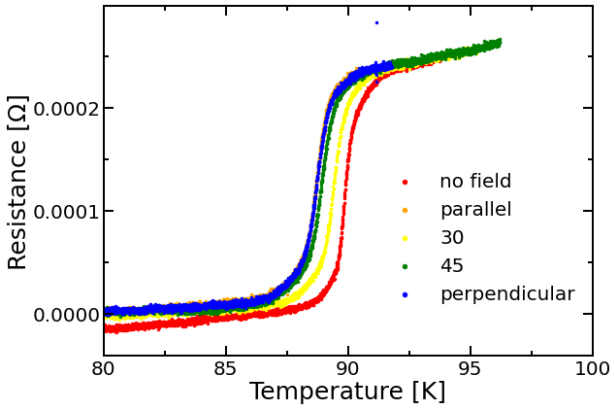

Figure 16: Shows the transition of the YBCO on the second bridge transitioning into the superconducting phase for different B field incident angles.

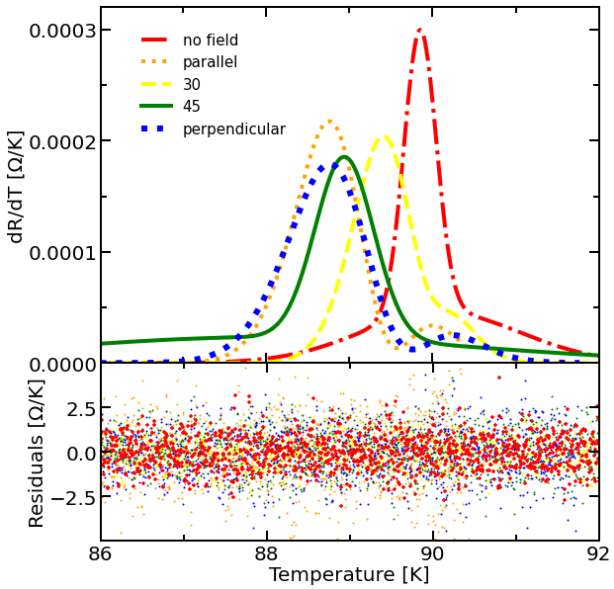

Figure 17: Shows the gradient of the transition for the second bridge curve-fitted to the double gaussian model, note the residuals are multiplied by 10^4

Experiment	Critical temperature [K]
No B field	90.9±0.5
Parallel	90.7±0.5
30	89.4±0.6
45	89.5±0.6
Perpendicular	89.8±0.6

Table 2: critical temperatures for No strain

Experiment	Critical Temperature [K]
No B field	90.0±0.4
Parallel	89.4±0.6
30	89.1±0.4
45	89.0±0.6
Perpendicular	88.8±0.5

Table 3: critical temperatures for First bridge

Experiment	Critical temperature [K]
No B field	90.0±1.0
Parallel	89.2±0.7
30	89.7±0.5
45	88.5±2.6
Perpendicular	89.3±0.8

Table 4: critical temperatures for Second bridge

Experiment Measurement	No Bridge Voltage[V]	First Bridge Voltage[V]	Second Bridge Voltage[V]
No Bfield (Hall probe with current)	(0.006182 ± 0.000001)	(0.004527 ± 0.000006)	(0.003635 ± 0.000006)
Perpendicular	(0.2897 ± 0.0003)	(0.27454 ± 0.00003)	(0.27607 ± 0.00005)
Parallel	−(0.001496 ± 0.000007)		(0.027841 ± 0.000004)
30 degrees	(0.1476 ± 0.0001)		
45 degrees roughly		(0.2139 ± 0.0002)	

Table 5: shows B field noise values recorded at the established angles, by Error Appendix 3

Gauss stick found maxima of (0.323 ± 0.005)T and $-(0.293 \pm 0.005)$T

date	a_0	a_1	a_2	a_3	a_4
01/03/2023	$-(212.2 \pm 0.3)$	(29.78 ± 0.04)	$-(1.213 \pm 0.002)$	(0.02328 ± 0.00003)	$-(0.0001664 \pm 0.0000007)$
06/03/2023	$-(732.2 \pm 0.1)$	(85.91 ± 0.01)	$-(3.456 \pm 0.0004)$	(0.063868 ± 0.000009)	$-(0.00043668 \pm 0.00000006)$
08/03/2023	$-(812.4 \pm 0.1)$	(94.97 ± 0.01)	$-(3.8674 \pm 0.0005)$	(0.07100 ± 0.00001)	$-(0.00048655 \pm 0.00000007)$
10/03/2023	$-(1271.0 \pm 0.3)$	(136.36 ± 0.03)	$-(5.226 \pm 0.001)$	(0.08976 ± 0.00002)	$-(0.0005759 \pm 0.0000001)$

Table 6: shows the curve-fit parameters of the forth order polynomial over 80-100K range

The 01/03 calibration was used for the no strain experiment. The 06/03 and 08/03 was used for the first bridge experiment. The 10/03 was used for the second bridge experiment.

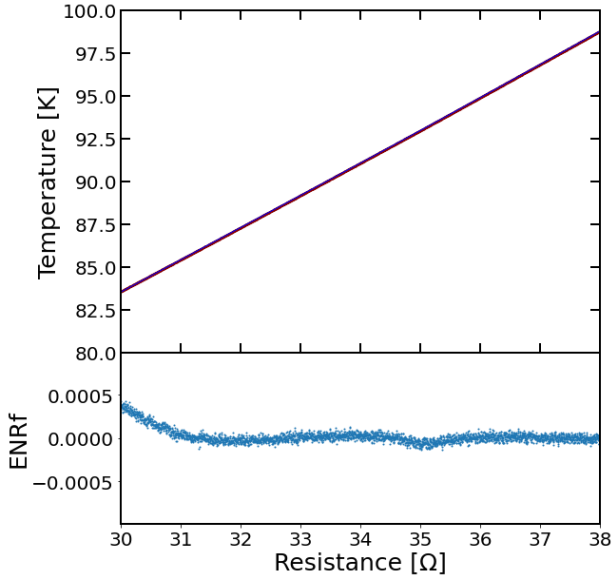

Figure 18: shows the temperature calibration for the no-strain experiment performed on the 01/03/2023.ENRf are error normalised residuals.

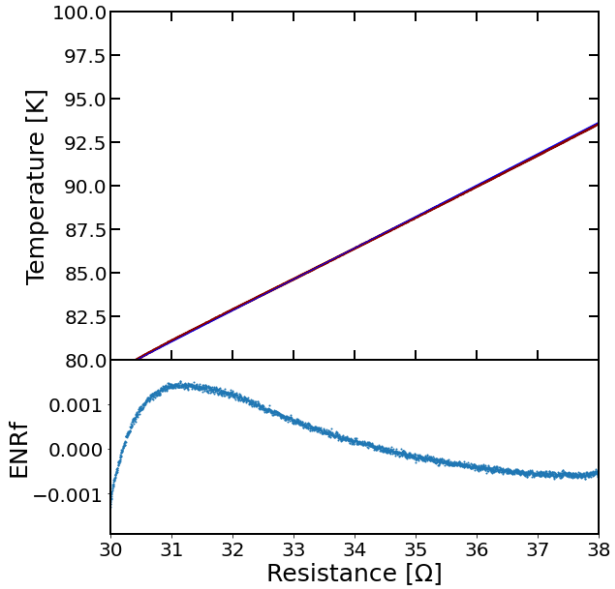

Figure 19: shows the temperature calibration for the first bridge performed on the 06/03/2023.ENRf are error normalised residuals

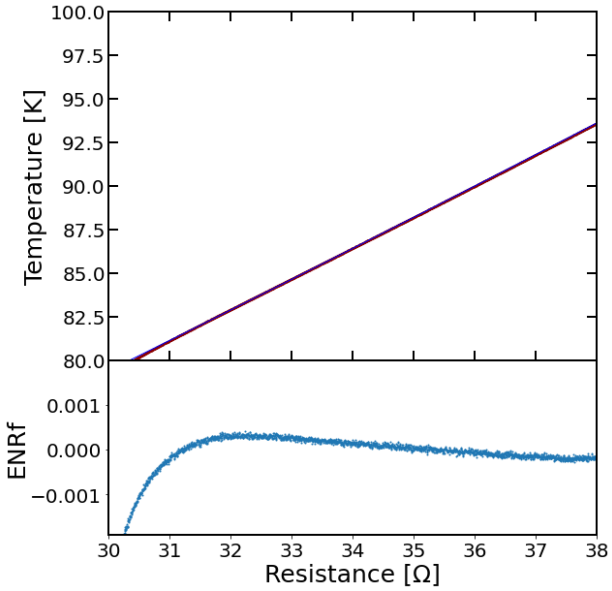

Figure 20: shows the temperature calibration for the first bridge performed on the 08/03/2023.ENRf are error normalised residuals

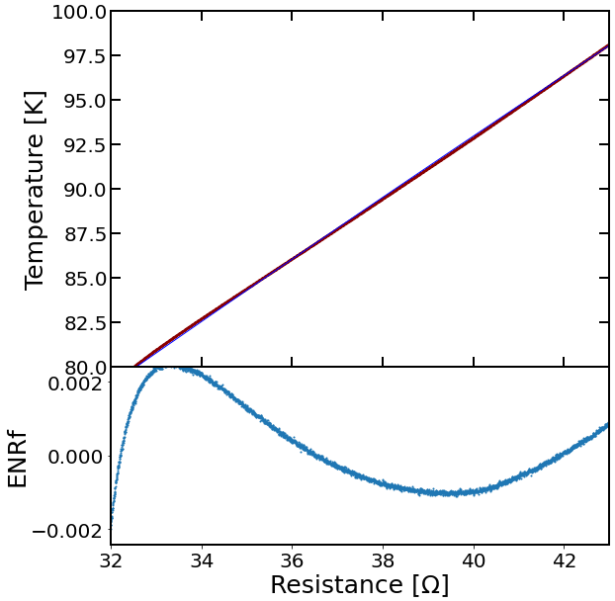

Figure 21: shows the temperature calibration for the second bridge experiment performed on the 10/03/2023.ENRf are error normalised residuals.

4. Discussion

All the experiments display superconductivity, as their resistances drop to near zero when they are at a temperature less than the critical temperature[2].
The 20 percent closed method was used in the no strain experiment and the 5 percent partially open was used in the rest of the experiments. This was due to a lack of ability to stabilize the dynamic equilibrium required for the 5 percent method. Overtime with practise it was mastered. The 5 percent method was superior because it collected more data, which could be better curve fitted. The one downside is that there more noise with this technique.
The critical temperature of YBCO is well defined and is given a literature value between 90-92K[2].

When No B field was applied, the strain did not affect the critical temperature[15][16], because the values in table 2, 3 and 4 all lie within error. The quasi-particles moving in the copper oxides planes in the superconducting phase interact on the microscopic scale. The smaller the radius of curvature the higher the bending strain. The bending strain applied is a macroscopic bulk property, that effects the structural integrity of the material, as opposed to the directly effecting the physics at the microscopic level, in no B field. This can be seen in the shape of the gaussians in figures 13, 15 and 17, they all have similar maximum gradients. However, differ slightly with the separation of their gaussians. Figure 15's no B field plot shows a clear split. Supplementary Appendix 3 provides the curve-fit parameters of the double gaussian and there a clear split in the gaussian's means when there is an applied strain. Also, an incident B field closer the maxima split the gaussians more. The physics of high temperature cuprate superconductors does not have a widely accepted consensus. A theoretical and simple explanation for the splitting of the double gaussian could be that there is an intermediate state that is a function of macroscopic bending strain, possibly a vortex mixed state. This intermediate state occurs between the normal phase and the superconducting phase. A pure phonon-electron theory of superconductivity does not work for high temperature superconductors, however phonons do contribute to their physics. A BCS theory perspective on this would be that when the YBCO strip has an applied strain this effects the crystal vibrations of the lattice. This causes the phonon-electron interaction to differ, resulting in a slightly different intermediate phase. When the maximum B field is applied, to the different strains, the critical temperature drops when it's under higher macroscopic strain. The critical temperature is affected by the incident B field angle because the YBCO is highly anisotropic. This is because of its dopants. The undisturbed CuO_2 plane, shown in figure 3, is a Heisenberg antiferromagnet and mott insulator. The CuO_2 plane is a mott insulator because all the electrons in the Cu-O-Cu pi bond, shown in figure 24, are localised in the covalent bonds, because of the strong coulomb potential. The electrons can only hop between the p orbitals of the Oxygen and the d orbitals of the Cu that overlap. The strong coulomb potential prevents electrons hopping between Cu sites, because the electrons must overcome a strong coulomb barrier and the localised electrons do not have that energy to do this, even at low temperatures. The two copper atoms contributing electrons to the oxygen atom must have opposite spins as it is in the ground state. Meaning the electrons in neighbouring atoms are antiferromagnetically aligned [15]. Conduction is not possible in this system. There are only localised electrons in the covalent bond and no free electrons. When the dopants are added this distorts the symmetry of the plane and adds a hole to the system. The electrons can now pass to Cu sites freely, this is shown in figure 2. This melts the anti-ferromagnetism. This hole moves around and is constantly being occupied, this causes new vacancies to appear. The electrons are no longer localised to the covalent bonds and are now delocalised. The delocalised electrons lie in the pi orbitals of the Cu-O-Cu ligands in x-y plane for YBCO, and can move to different Cu sites when there is a neighbouring hole. They are not quite free but they can be described that way. The superconductivity of YBCO is therefore two dimensional. This is why anisotropy is seen when B field angle is varied. The experiments with the higher B field intensity on the Copper oxide plane cause a lower critical temperature. This is observed for all strains.

YBCO is not an isotropic material (breaks rotational symmetry). Its delocalised electrons can only move in the x-y copper oxide plane. Therefore, this direction of the lattice shows predominant superconductivity. In the z direction there is small amounts of superconductivity. The layers of copper oxide are electronically isolated from each other.

When the YBCO is cooled below its critical temperature quasi-particles form. There is an attractive interaction that is stronger than the coulomb repulsion between the fermions that pair. There is a debate whether it is holes or electrons that form these quasi-particles in YBCO. The conception of the cooper pair has been around since 1972, but the cooper pair has not been observed.

The experimental stick can be modelled as a rigid rod with six degrees of freedom DOF, 3 rotational and 3 translational. The experiment can be simplified by constraining irrelevant degrees of freedom. The translational degrees of freedom can be removed because of the Gauss stick experiment. It was found that raising and lowing the Gauss stick by 1cm each way, did not affect the magnitude of the B field on the Gauss meter recording. Its effect was less than the resolution of the Gauss meter. This implied that the translational DOF's effect , for the YBCO strip, is negligible for small displacements. This reduces the experimental degrees of freedom from 6 to 3. (Supplementary appendix 4)

The Knock test also verified this by showing that the reposition test contributed an error in angle 10 times larger, by Error Appendix 3. The main source of error comes from the ϕ angle between the B field and the Copper oxide layers of the YBCO, not the translational position of the YBCO. The experiment can be reduced to the 3 angular degrees of freedom.

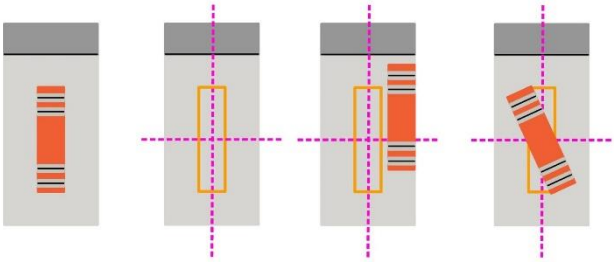

Figure 22: shows different variations of YBCO positions on the experimental stick's head

The first three arrangements are allowed, as the translational displacement was shown to have a negligible effect on the incident B field. The angular position relative to the normal configuration in figure x is important because when the experimental stick is rotated, the flux travelling through it at different angles will be inconsistent with other experiments. The bridge prevented the YBCO slipping out of line, with the experimental stick's axis.

During the non-strain experiment the YBCO was positioned in line with this axis. The experiment can be reduced to two angular degrees of freedom.

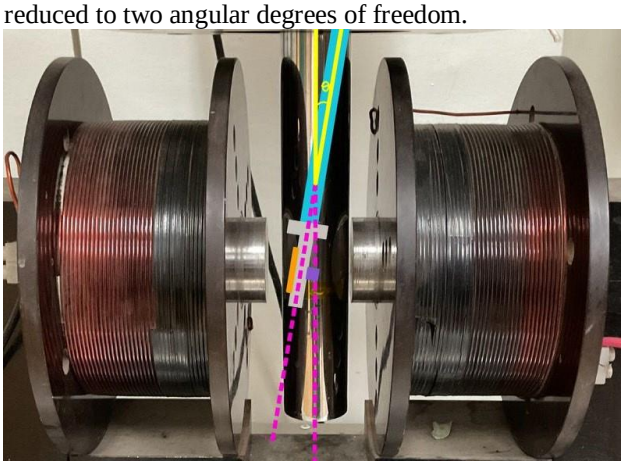

Figure 23: shows the azimuthal angle of the experimental stick axis and axis of the chamber.

This azimuthal angle is negligible in the experiment as the experimental stick it is held in a tight fixed position with a clamp. As a result, this experiment has One dominant DOF, the angle of the YBCO copper oxides layers to the B field (figure 6).

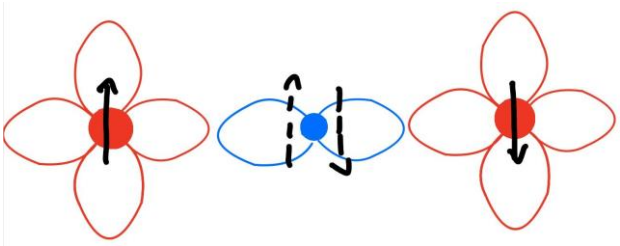

Figure 24: shows the spins of a pi bond, red is copper and blue is oxygen.

Figure 24 shows the antiferromagnetism of a bond when the electrons are localised.

When new strains were used, components were resoldered back on the experimental stick, this would give a different noise to that component. This another reason why the temperature needed to be recalibrated.

Figures 18,19,20,21 show that the errors in the temperature calibrations got larger as the experiment continued. Just as the experimental method was improving. This is due to damage to sensitive platinum thermometer. Each experiment required a new overnight temperature calibration because the physical environment inside of the cryostat was different.

It can be seen in figure 23 that the chamber does not lie equidistant between the coils.
In addition to this the cryostat chamber was surrounded by an iron core, which would magnetise when a B field is applied. Also, the number of coils was not known.
The maxima recorded by the gauss probe had values of (0.323 ± 0.005)T and $-(0.293 \pm 0.005)$T. The maxima have a 10% difference. This is because the chamber does not lie equidistant between the electromagnetic coils.

All of these uncertainties in B field strength, as well as the lack of B field noise recordings, make it hard to compare different B field angles.

It's difficult to compare the data from the first and second bridges because the first bridge had a higher strain than the second and the first bridge was experimented on first. We didn't have enough time to repeat the experiment without strain to see if it damaged the superconductivity of the tape. The largest source of error was in the ϕ angle, this was shown in Error Appendix 5A. Along with this, B field noise measurements where not taken after every experiment. That is why some cases shown in figures 12, 14 and 16 show some instances with smaller angles having higher critical temperatures than larger angles. This is because of the repositioning error. This ties into the point that the method was developed over time and significantly improved at the end of the lab.

5. Conclusions

The strain deforms the YBCO strip macroscopically. This effects the phonon-electron interactions and pulls the double gaussians further apart for a high bending strain[15][16]. The gaussians were also pulled further apart when a stronger incident B field is acting on the Copper oxide layers. This is because the superconductivity if more prevalent in the Copper oxide plane. The B field also lowers the critical temperature by approximately a degree. The B fields used in this experiment had a lot of issues and was difficult to model, but a pattern of behaviour was seen. The critical temperatures calculated lie within error of the literature values[2]. The lack consensus for the theory behind the cuprate superconductors leaves a mystery behind the results. The BCS theory cannot fully explain the cuprate superconductors as their temperatures are too high, however the existence of the superfluid cooper pair can be used to explain the near zero resistance in the YBCO when it transitions into the superconducting phase. It fails to explain the two dimensionality of the YBCO's superconductivity. If there was more time the experiment would be repeated with accurately collected B field noise measurements and also the YBCO would be tested to see if there was any damage to its superconductivity after experiencing strain. The Degrees of freedom of the experimental stick can be reduced from 6 DOF to 1 DOF. This explains the result of the repositioning test. The repositioning tests shows that the error in repositioning the experimental stick to a maximum is 10 times larger than the error associated knocking the apparatus repeatedly.
The largest contribution to error was the angle between the B field and the Copper oxide plan.

References

[1] H. Onnes, *BSPS volume 124*, Boston Studies in the Philosophy of Science book series, 1991, chapter named *Further experiments with Liquid Helium. G. On the Electrical Resistance of Pure Metals, etc. VI. On the*

Sudden Change in the Rate at which the Resistance of Mercury Disappears
[2] R. Combescot, *SUPERCONDUCTIVITY An Introduction,* Cambridge University Press, Cambridge, p1-6
[3] L. Cooper, *BCS: 50 years*, World Scientific Publishing Co. Pte. Ltd, 2010, pg 35-40
[4] J. Bardeen, L. Cooper and J. Schrieffer, *Theory of Superconductivity,* American Physical Society, 1957
[5] R. Combescot, *SUPERCONDUCTIVITY An Introduction,* Cambridge University Press, Cambridge, p7-8
[6] M. Zhitomirsky, *Ginzburg-Landau theory of vortices in a multigap superconductor,* American Physical Society, 2004
[7]http://past.ieeecsc.org/pages/nobel-laureates-superconductivity#:~:text=In%201972%2C%20John%20Bardeen%2C%20Leon,usually%20called%20the%20BCS%20theory.%22, 2023
[8] R. Combescot, *SUPERCONDUCTIVITY An Introduction,* Cambridge University Press, Cambridge, p28
[9]File:Ybco.jpg - Wikimedia Commons, 2023
[10] Y.Nambu, *Quasi-Particles and Gauge Invariance in the Theory of Superconductivity,* American Physical Society, 1960
[11] Y. Kharkov, *The amplitudes and the structure of the charge density wave in YBCO,* volume 6, scientific reports, 2016

[12] J .Halbritter, *A review of weak/strong links and junctions in high-T_c superconductors as a transition to a Mott insulator,* IOP Publishing Ltd, 2003

[13] F. McCrackin, *Simple calibration procedures for platinum resistance thermometers from 2.5 to 14 K,* Review of Scientific Instruments **46**, 550, 1975

[14]J.rojas, *Pairing and Coherence Transition in La1.82Sr0.18CuO4 Strongly Two-Dimensional Superconductor, Brazilian journal of physics, 2006*
[15] Y. Jingfeng, *Macroscopic residual stress and properties in different YBa2Cu3O7-x heterogeneous systems,* Physica C Superconductivity, 2020
[16] S. Favre, Depression of critical temperature due to residual strain induced by PLD deposition on *YBa2Cu3O7-x thin films,* Materials Chemistry and Physics, 2021

[17] I. Hughes, *Measurements and their Uncertainties A Practical Guide to Modern Error Analysis*, OXFORD UNIVERSITY PRESS, Oxford, pg 44
[18] I. Hughes, *Measurements and their Uncertainties A Practical Guide to Modern Error Analysis*, OXFORD UNIVERSITY PRESS, Oxford, pg 6
[19] I. Hughes, *Measurements and their Uncertainties A Practical Guide to Modern Error Analysis*, OXFORD UNIVERSITY PRESS, Oxford, pg 16
[20] I. Hughes, *Measurements and their Uncertainties A Practical Guide to Modern Error Analysis*, OXFORD UNIVERSITY PRESS, Oxford, pg 72-77
[21] I. Hughes, *Measurements and their Uncertainties A Practical Guide to Modern Error Analysis*, OXFORD UNIVERSITY PRESS, Oxford, pg 40-42

Error Appendix

Error Appendix 1: Error in the platinum thermometer resistance

The temperature model in eq(2) is a function of the platinum thermometers resistance [17].

$$\alpha_V = \sqrt{(\alpha_V^{Noise})^2 + (\alpha_V^{Precision})^2 + (\alpha_V^{Accuracy})^2} \quad \text{eq(5)}$$

$$\alpha_I = \sqrt{(\alpha_I^{Noise})^2 + (\alpha_I^{Precision})^2 + (\alpha_I^{Accuracy})^2} \quad \text{eq(6)}$$

The errors of the Precision, noise and accuracy where added in quadrature.

The error in the precision of the experiment was half the resolution of the Keithley 2000 [18].

$$\alpha_V^{Precision} = (5 \times 10^{-7})V$$
$$\alpha_I^{Precision} = (5 \times 10^{-7})A$$

The calibration was performed with data, collected between the 80-100K temperature range, from the Mercury ITC. The Noise errors for the platinum thermometer were the standard errors in the voltages, V and currents, I recorded by the keithley 2000, when the power supply to the platinum thermometer was switched off.

The accuracy error was the standard errors in the voltages and currents recorded when the experimental current was passing though the platinum thermometer.

The equation for standard error[19], α is

$$\alpha = \frac{\sigma_{N-1}}{\sqrt{N}} \quad \text{eq(7)}$$

Where σ_{N-1} is the sample standard deviation and N is the population size between the temperature range of 80-100K.

Calibration date	α_V^{Noise},[V]	α_I^{Noise},[A]	$\alpha_V^{Accuracy}$,[V]	$\alpha_I^{Accuracy}$,[A}
01/03/2023	4×10^{-7}	5×10^{-7}	1×10^{-5}	5×10^{-8}
06/03/2023	4×10^{-7}	5×10^{-7}	2×10^{-5}	6×10^{-8}
08/03/2023	5×10^{-7}	5×10^{-7}	2×10^{-5}	2×10^{-8}
09/03/2023	4×10^{-7}	5×10^{-7}	3×10^{-5}	4×10^{-8}

Table 7: Shows the associated errors that arise in the current and voltage measurements of the platinum thermometer.

Below Is the equation for Resistance, R and its error [9].

$$R = \frac{V}{I} \quad \text{eq(8)}$$

$$\Rrightarrow \alpha_R = \bar{R}\sqrt{(\frac{\alpha_I}{I_{min}})^2 + (\frac{\alpha_V}{V_{min}})^2} \quad \text{eq(9)}$$

Where the I_{min} and V_{min} are the minimum voltages amd currents recorded between the 80-100K modelling region to maximise the error. $\bar{R}$ is the average Resistence in the region, this will provide a rough order of magnitude in the error of our resistance, which can be used in the curve-fit of the model against the Temp ITC data.

Calibration date	Bridge	α_R,[Ω]
01/03/2023	No Bridge	2×10^{-4}
06/03/2023	Bridge 1	4×10^{-4}
08/03/2023	Bridge 1	4×10^{-4}
09/03/2023	Bridge 2	10^{-3}

Table 8: shows the error in the platinum thermometer resistance.

Error Appendix 2: Error of Temperature Calibration Curve-fit, procedure

To find the error in the curve-fit associated errors find the minimum of the error surface resulting from the curve-fitted parameters [20], Addressed in Supplementary appendix 3. The error in a given parameter a_j of the eq(2) will be

$$\alpha_{a_j} = \sqrt{\frac{2}{\left(\frac{\partial^2 \chi^2}{\partial a_j^2}\right)}} \quad \text{eq(10)}$$

to calculate the error in temperature predicted by the temperature calibration a functional approach was taken. For more information about this derivation read Supplementary Appendix 5

The forth order model has parameters, a_0, a_1, a_2, a_3 and a_4

The function T(R) can be rewritten as

T(R, a_0, a_1, a_2, a_3, a_4)

The error in temperature as a result of the a_j parameter for a given Resistance R_i is [11]

$$\alpha_{T(R_i)}^{a_j} = \left|T\left(R_i, \dots, a_j + \alpha_{a_j}, \dots\right) - T\left(R_i, \dots, a_j, \dots\right)\right| \quad \text{eq(11)}$$

Adding the errors in quadrature gives the total area squared

$$\alpha_{T(R_i)}^2 = (\alpha_{T(R_i)}^{a_0})^2 + (\alpha_{T(R_i)}^{a_1})^2 + (\alpha_{T(R_i)}^{a_2})^2 + (\alpha_{T(R_i)}^{a_3})^2 + (\alpha_{T(R_i)}^{a_4})^2 \quad \text{eq(12)}$$

The square root of the sum gives the error in temperature at a specific Resistance that is plugged into the calibration.

$$\alpha_T^{Calibration} = (\alpha_{T(R^{average}_{})}) \quad \text{eq(13)}$$

The average R is used to find the error[21]

Error Appendix 3: Error in Angle of B field

As mentioned before the DOF of the rigid rod can be reduced from 6 to 1.

Noise recordings for the Hall probe where taken with no applied B field, perpendicular, parallel, 30 degrees and 45 degrees. The angles where marked with a white strip and colour coded so the measuring stick could be rotating to get data for multiple angles during a lab session.

Firstly, there is noise in the Hall probe, which is recorded in No B field. The mean Voltage was taken over a 15-minute period and was taken away from a new voltage recording to provide an updated corrected accurate recording, which shifts it.

$$V_{Hall\ probe}^{Corrected} = V_{Hall\ probe}^{Recorded} - \overline{V_{Hall\ probe}^{No\ field}} \quad \text{eq(14)}$$

The maxima was calculated from the 360 rotation and for angle ϕ as shown in figure 7.

And the angle required was converted to a voltage

$$\phi = cos^{-1}\left(\frac{V^{recorded} - \overline{V_{noise}}}{V_{Max} - \overline{V_{noise}}}\right) = cos^{-1}\left(\frac{V^{Corrected}}{V_{Max}^{Corrected}}\right) \quad \text{eq(15)}$$

This Derivation is in Supplementary Appendix 4.

Knocking the table (does it support the suggestion that reduces the degrees of freedom)

The error in the corrected hall prove voltage is[17]

$$\alpha_V^{Corrected} = \sqrt{\left(\alpha_V^{No\ Bfield}\right)^2 + (\alpha_V^{Recorded})^2} \quad \text{eq(16)}$$

Which is just the quadrature sum of the standard error[19] in the noise for the No-field experiment and the recorded experiment.

$$\alpha_V^{Recorded} = \frac{\sigma_{N-1}^{Recorded}}{\sqrt{N}} \text{ eq(17)}$$

And

$$\alpha_V^{No\ Bfield} = \frac{\sigma_{N-1}^{No\ Bfield}}{\sqrt{N}} \text{ eq(18)}$$

Where N is the population size of the data collected over the noise recording, for each respective recording.

Error appendix 4: error in critical temperature

$\alpha_{T_c} = \sqrt{\sigma_1^2 + \sigma_1^2}$ eq(19)

The error was chosen as standard deviations reperesent distributions[17]

Error Appendix 5: tests which contribute to error.

Part A: Repositioning

This test relies on the consistency of the experimentalist. Hall probe does not work at low temp so we had to use markers.

First the corrected maxima (perpendicular angle) is recorded and a white line is marked on the black clamp attached to 5 on the cryostat in figure 6. The experimental stick is rotated out of position and it repositioned to the original mark.

The fractional uncertainty of the old and new maximums where calculated.

$$V_{initial}^{Max} = (0.2828 \pm 0.0001)V$$
$$V_{final}^{Max} = (0.2777768 \pm 0.000004)V$$

By Error Appendix 3 and Supplementary Appendix 4.

Therefore the fractional uncertainty is

$$\frac{\left|V_{final}^{Max} - V_{initial}^{Max}\right|}{V_{initial}^{Max}} \approx 0.02$$

and the order of magnitude of the voltage change was

And the order of magnitude of the voltage change was ≈0.01V

This would give an approximate angle change of

$$\frac{\pi}{2} - cos^{-1}\left(\frac{0.01}{0.2828}\right) \approx (4 \times 10^{-2}) \text{ rads}$$

Part B: Knocking the table (translational DOF mostly, some angular effect).

This test was performed when the YBCO was laying on the first bridge. The maxima (perpendicular position) voltage was recorded and then the table housing the cryostat was given a harsh nudge (they where corrected) as mentioned in other appendices. The difference between the new and old maxima gives the order of magnitude a knock to the equipment gives. The voltages where averages. This difference in an Voltage they where corrected by the way can be converted to an angle using…

$$V_{initial}^{Max} = 0.278720\ V$$
$$V_{final}^{Max} = 0.277768\ V$$

Therefore the fractional error was

$$\frac{\left|V_{final}^{Max} - V_{initial}^{Max}\right|}{V_{initial}^{Max}} \approx 0.003$$

And the order of magnitude of the voltage change was ≈0.001V

This would give an approximate angle change of

$$\frac{\pi}{2} - cos^{-1}\left(\frac{0.001}{0.27872}\right) \approx (4 \times 10^{-3}) \text{ rads}$$

This angle change is 10 times smaller than repositioning supporting removing the translational degrees of freedom. what is more correct analysis of this difference in angle

Supplementary Appendix

Supplementary Appendix 1: derivation of diamagnetism within a superconductor

For a superconductor in conditions that obey the Meissner effect B= 0 under an applied magnetic field H. The magnetisation M of the superconductor is

$$M = \chi H \text{ eq(20)}$$

This implies that, using eq(1)

$$B = \mu_0(H + M) = \mu_0(1 + \chi)H = 0$$

Where μ_0 is the permeability of free space. So, the magnetic susceptibility χ = -1. A superconductor is therefore a perfect diamagnet.

Supplementary Appendix 2: Circuit diagrams for the experimental stick.

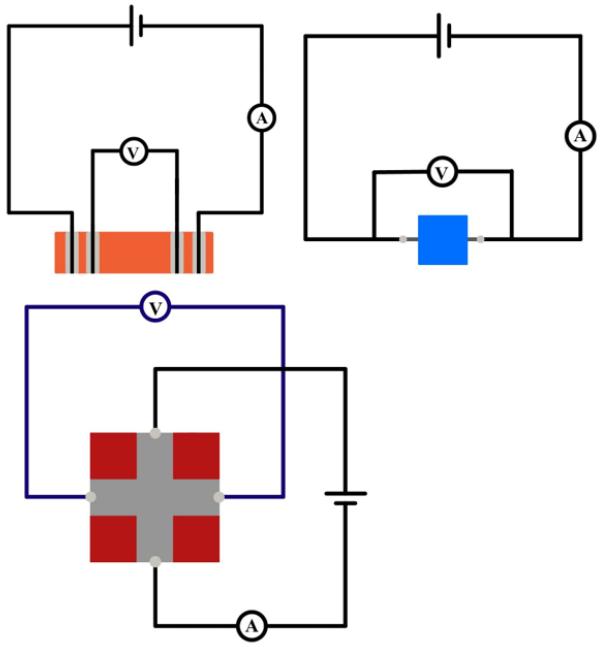

Figure 25,26,27: show the circuits wired for the YBCO (top left), platinum thermometer(top right) and Hall probe (bottom).

Supplementary Appendix 3: normal varnishing method

To attach these components to the experimental stick first apply varnish to the experimental stick's head and stick the insulating rizzler paper to it. Then apply vanish again to the corresponding component such as the YBCO tape, bridge, hall probe etc and stick it on the rizzler paper. Wear gloves when handling varnish. Place the experimental stick in a fumes cupboard and leave it for a day to set.

Supplementary Appendix 3: Double gaussian tables

Experiment	μ_1	σ_1	a_1	μ_2	σ_2	a_2
No Bfield	90.6233 +- 0.0002	0.1648 +- 0.0003	0.000263 +- 1e-06	91.147 +- 0.001	0.4455 +- 0.001	0.0001488 +- 2e-07
Parallel	90.66 +- 0.04	0.37 +- 0.03	0.08 +- 7.28	90.66 +- 0.04	-0.37 +- 0.03	-0.08 +- 7.28
30	89.169 +- 0.001	-0.321 +- 0.003	-0.000129 +- 3e-06	89.633 +- 0.004	-0.487 +- 0.001	0.000301 +- 2e-06
45	89.481 +- 0.006	-0.447 +- 0.002	0.0 +- 6.0	89.481 +- 0.006	-0.446 +- 0.002	-0.0 +- 6.0
perpendicular	89.93 +- 0.003	0.544 +- 0.002	8.6e-05 +- 1e-06	89.6817 +- 0.0004	0.272 +- 0.001	0.00023 +- 1e-06

Table 9: These are the constants from the gaussian curve fit on the gradient of the data from the experiment with no strain

Experiment	μ_1	σ_1	a_1	μ_2	σ_2	a_2
No Bfield	89.97 +- 0.03	0.29 +- 0.03	0.04 +- 1.93	89.97 +- 0.03	0.29 +- 0.03	-0.04 +- 1.93 -0.0 +- 0.1 - 4.08e-
Parallel	89.212 +- 0.001	-0.5205 +- 0.003	0.000278 +- 1e-06	89.4498 +- 0.0006	0.3396 +- 0.007	-0.0001653 +- 1e-06
30	88.802 +- 0.0003	0.3859 +- 0.003	0.0001921 +- 1e-07	89.4931 +- 0.0008	-0.1949 +- 0.007	3.38e-05 +- 1e-07
45	88.98 +- 0.05	0.45 +- 0.03	0.0 +- 0.1	88.98 +- 0.05	0.44 +- 0.03	-0.0 +- 0.1
perpendicular	88.5583 +- 0.0002	0.4556 +- 0.002	0.0001916 +- 1e-07	89.0193 +- 0.0003	0.0956 +- 0.004	-4.08e-05 +- 1e-07

Table 10: These are the constants from the gaussian curve fit on the gradient of the data from the first bridge

Experiment	μ_1	σ_1	a_1	μ_2	σ_2	a_2
No Bfield	89.851 +- 0.001	0.193 +- 0.002	0.000255 +- 2e-06	90.1 +- 0.02	0.95 +- 0.03	4.6e-05 +- 1e-06
Parallel	89.071 +- 0.01	-0.559 +- 0.003	0.00032 +- 1e-05	89.359 +- 0.005	0.354 +- 0.007	-0.00024 +- 1e-05
30	89.6 +- 0.01	0.455 +- 0.005	0.00027 +- 1e-05	89.85 +- 0.01	-0.28 +- 0.01	-0.00014 +- 2e-05
45	88.941 +- 0.004	0.351 +- 0.005	0.000164 +- 2e-06	88.0 +- 0.6	-2.6 +- 0.5	2.3e-05 +- 2e-06
perpendicular	89.13 +- 0.02	0.66 +- 0.01	0.00026 +- 1e-05	89.48 +- 0.01	0.43 +- 0.01	-0.00019 +- 1e-05

Table 11: These are the constants from the gaussian curve fit on the gradient of the data from the second bridge

Supplementary Appendix 4: translational motion in the x-y plane of the experimental stick

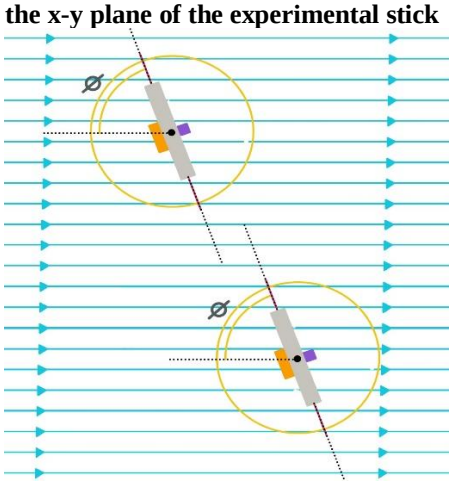

Figure 28: illustrates two "experimental sticks" with a translational transformation in the x-y plane

Supplementary appendix 5: Method of least squares
Curve fitting the 4th order resistance polynomial to the Temperatures T_i of ITC from 80-100K.

Simplified method [20]

1) For each Resistance R_i collected calculate the temperature value $T(R_i)$ from the eq(2)
2) For all R_i values, calculate the square of the normalised residual.

$$\left[\frac{(T_i - T(R_i)}{\alpha_R}\right]^2 \quad \text{eq(21)}$$

Where α_R was calculated in Error Appendix 1.

3) Find the Chi-square χ^2 by summing the squares of the normalised residuals over the T_i from 80-100K
4) Finally minimise χ^2 by optimising the curve-fit parameters.

Scientific Summary for a General Audience

Lorem ipsum dolor sit amet, consectetur adipiscing elit. Praesent lacus lectus, elementum sagittis eros in, molestie aliquam sapien. Curabitur viverra eros sed nulla mattis aliquet. Aliquam ullamcorper metus vitae feugiat vulputate. Aliquam sed ultrices ipsum, quis vulputate tellus. Quisque cursus nisl ac orci posuere, vitae posuere sem elementum. Fusce ultrices nibh arcu, sed malesuada orci ullamcorper a. Fusce id aliquet nisi. Mauris in mollis turpis. Ut vestibulum est erat, quis vulputate orci pretium eget. Fusce nec tincidunt lacus.

Fusce aliquam ligula vitae nisl aliquam aliquet. Mauris pellentesque quam quis est porta, at imperdiet tellus ornare. Nam dapibus enim quam, et faucibus dolor egestas ut. Quisque eu sem maximus, faucibus lectus eu, sagittis ex. Etiam luctus, nulla ut pretium iaculis, magna augue lobortis metus, at blandit arcu mauris ac eros. Suspendisse justo libero, consequat aliquet porttitor a, suscipit non felis. Aliquam non auctor diam. Donec interdum metus a accumsan tempor. Phasellus commodo facilisis sem, vel finibus nisi. Vivamus est odio, sagittis nec ex ut, eleifend maximus velit. Phasellus in vehicula lectus. Proin ornare mauris ut pellentesque tempus.